Particle Acceleration at Perpendicular Shocks: The Role of Field Line Topology

József Kóta*

*University of Arizona, Lunar and Planetary Laboratory, Tucson, AZ 85721-0092, USA

***Abstract*. Particle acceleration at 2-D shocks can quite differ from our expectation based on 1-D shocks. We discuss several features of 2-D shocks. First, we present a simple example of diffusive acceleration and demonstrate that (1) 'hot spots' and cold regions can be expected along the shock face, as the field line configuration changes, (2) the flux of accelerated particles (even the average flux) can be expected to increase beyond the shock, and (3) 2-D structure may lead to a softening of the spectrum.**

Next, we consider quasi-perpendicular shocks and discuss what happens when a field line is hit by a curved shock or is detaching from a shock. This mechanism is of interest on both large and small scales. We assume purely field aligned transport and address both the diffusive (large scale) and scatter-free (small scale) cases, looking from the perspective of one field line. We find that quasi-trapping of particles in front of the shock can lead to rapid and effective acceleration via multiple mirroring on the ever faster moving shock. This mechanism may be of importance at various astrophysical, heliospheric and CME-driven shocks.

***Keywords*: Acceleration, perpendicular shock, magnetic topology,**

I. Introduction

Much of our perception and expectation for shock acceleration is based on 1-D shocks. In reality, however, there are significant variations along the shock face. For instance, magnetic field lines can and frequently do intersect the shock more than once. This is one feature that cannot be modeled in 1-D, and leads to quite significant effects in 2-D or 3-D. Voyager observations provided clear examples that we need 2-D modeling. The spectrum of anomalous cosmic rays (ACRs) did not unfold at the termination shock (TS) and ACR flux continued to increase beyond the TS [1] [2]. This seemingly surprising finding can be interpreted as a natural consequence of magnetic topology at the TS [3],[4],[5].

In section II we consider a simple, transparent illustrative large-scale example of a 2-D shock with longitudinal structure along the shock face. We present analytical approximations and numerical simulations to demonstrate that the efficiency of acceleration may change quite dramatically along the shock. Cold regions are expected at places where the field line cross into the downstream region but soon recross the shock back to the upstream region. The opposite configuration, on the other hand, leads to an effective acceleration producing hot spots along the shock [5],[6]. Similar topological effects may be quite important at other shocks, too. They can appear on various scales, starting from large-scale, global structures of the TS [7], [4], down to smaller scales. Shocks are, in general, not ideal planes, but significant ripples occur [8],[9].

Section III discusses, in some detail, what happens when a curved shock hits a field line. By contrast with earlier studies [10],[11], [12], [13], we present an approach from a field-line perspective. We address both diffusive and scatter-free cases, considering purely field-aligned transport, which represents a singular case in the diffusive description. We find that rapid acceleration is possible through multiple mirroring at the stronger downstream field. This mechanism can conceivably play role at number of scenarios.

II. Illustrative Example of a 2-D Shock

The blunt termination shock is crossed by the spiral field lines multiple times as the field/shock orientation changes [14], [7]. A 2-D shock with such a structure along the shock face cannot be expected to give a uniform power-law ACR spectrum [3], [4]. In this section, we consider a simple, analytically tractable case which captures the important topological effects. Other aspects of a 2-D shocks were discussed in [15] and [16]. Here, we assume a planar shock and a magnetic field (red lines in Figure 1.) with alternating direction along the shock. Assuming periodic boundary condition, this scenario resembles the blunt TS: places where field lines first/last hit the shock can be perceived as the nose/tail directions.

It is clear that, even without considering drift into the third direction, the diffusion coefficient κ_{xy} changes along the shock hence the well-known solution of the 1-D planar shock will be modified, and this modification can be quite significant. Roughly speaking, the upstream parallel diffusive streaming, flowing away from the shock changes direction causing flux enhancements or reductions at the places where the field lines turn.

In the simulation presented in Figure 1, we use a small perpendicular diffusion coefficient, with $\kappa_\perp = 0.01\kappa_\parallel$. The upstream shock angle is $\Theta_{Bn} \approx 5^o$. A further dimensionless parameter is $VY/\kappa_\parallel = 0.1$, where V is the upstream wind speed, while Y is the length of period along the shock front. Particles are injected uniformly along the shock. At low energies, close to the injection energy, the fast local acceleration results in a more or

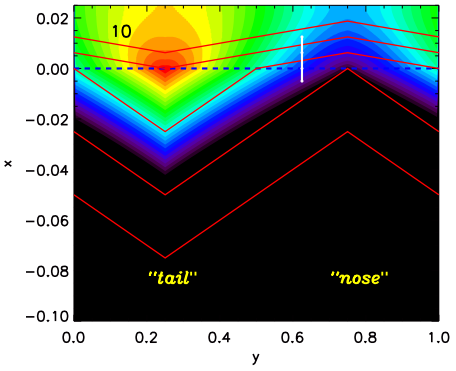

Fig. 1. Illustrative example of particle acceleration at a 2-D shock: the field (red line) is assumed to change direction periodically along the shock face. Accelerated particle fluxes (10 times of injection speed) are organized by the magnetic field, creating 'hot' and 'cold' spots, in the 'tail' and 'nose', respectively (see text).

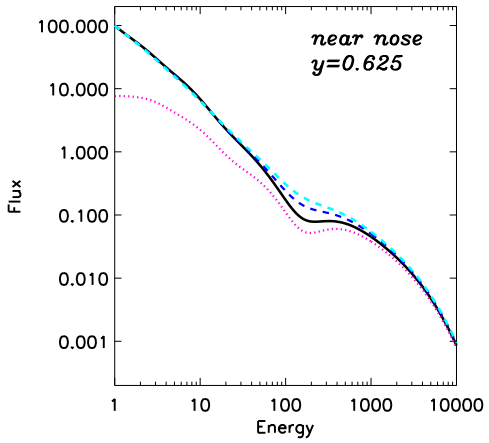

Fig. 2. Evolution of the energy spectrum while moving across the shock at $y = 0.625$ (white bar in Fig. 1). The spectrum is depleted at the shock (solid line), and unfolds gradually downstream (dashed lines). Dotted line indicates modulated spectrum upstream.

less uniform distribution along the shock. Toward higher energies (10 times injection speed shown in Fig. 1.), on the other hand, particle distribution tends to follow the magnetic field, rather than the shock. This results in "hot" and "cold" places along the shock front. The "cold" spot is the place where the field lines first hit the shock, which would correspond to the nose of the TS.

The simplicity of the model allows analytical approximation. In the absence of adiabatic cooling, Parker's diffusive transport equation [17] reduces to:

$$-\frac{\partial}{\partial \xi_i}\kappa_{ij}\frac{\partial f}{\partial \xi_j} + V_j\frac{\partial f}{\partial \xi_j} = 0 \qquad (1)$$

where, $\xi_i = (x, y)$, x points in the wind direction, and y points along the shock-face. Acceleration at the shock is treated as matching condition. In our simple case, all elements of the diffusion coefficient, κ_{ij}, are constant except that the sign of κ_{xy} (and κ_{yx}) alternates between the two regions. This permits the solution of $S_i = -V_i f$, where the diffusive streaming, and S_i has no component in the y direction along the shock ($S_y = 0$).

Now, assuming that the diffusion coefficient κ_{ij} is independent of momentum upstream, and vanishes downstream, the jump condition leads to the analytical solution:

$$f(\xi_i, p) \propto (p/p_0)^{-\gamma} \times exp\int^{\xi_i} d\xi_i' \kappa_{ij}^{-1} V_j \qquad (2)$$

with $\gamma = 3s/(s-1)$, where s stands for the shock ratio.

By contrast with the pure 1-D case, the solution (2) exhibits a remarkable structure along the shock face. The alternating non-diagonal element of the inverse tensor, κ_{yx}^{-1} results in a lateral gradient:

$$\frac{\partial ln\, f}{\partial y} = (1 - \frac{\kappa_\perp}{\kappa_\parallel})\,\frac{V}{\kappa_\perp}\, sin\Theta_{Bn}\, cos\Theta_{Bn} \qquad (3)$$

The above analytical solution assumes a shock which is perpendicular on average. Then, eq.(2) represents the asymptotic high-energy solution, toward which the distribution tends from the low-energy solution, determined by the injection profile along the shock. A uniform injection will result in a more or less uniform distribution at low energies, which should gradually converge to (2) toward high energies.

Solution (2) remains a usaful approximation, guiding our insight, if we relax our restrictions and permit κ_{ij} to depend on momentum, p, and remain finite downstream. Then, diffusion along the field behind the shock relaxes gradients and the lateral distribution eventually becomes more uniform. As a consequence, particle flux in the depleted 'nose' region increases beyond the shock. The spectrum, which starts as a power law everywhere, becomes steeper in the nose region, and less steep in the tail region as the spatial distribution adjust to (2). At still higher energies, diffusion becomes easier and the lateral variation decreases again.

Model simulations confirm these qualitattive expectations. Figure 2 shows how the energy spectrum may evolve as an observer moves from upstream to downstream in the nose area (at $y = 0.625$, indicated by white bar in Fig. 1.). The spectrum, which is depleted at the shock, will gradually unfold as the observer advances deeper downstream.

General considerations reveal further implications for 2-D shocks. Consider, for instance, the mean intensity $F(x, p) =< f >$ by averaging over y along the shock. After a straightforward manipulation, we arrive at

$$F(0, p) = F_\infty(p) + \frac{\kappa_{xy}}{\kappa_{xx}}\int_0^\infty \frac{\Delta f}{\Delta y} exp(-\frac{Vx}{\kappa_{xx}})\, dx \qquad (4)$$

where Δf refers to the difference between between the intensity maximum and minimum on a half period span $\Delta y = Y/2$. Eq. (4) implies that the mean downstream flux rises away from the shock. This, in turn, will also imply some softening of the spectrum w.r.t. plane shock. A straightforward calculation yields

$$\gamma = -\frac{\partial ln\, F}{\partial ln\, p} = \frac{3s}{s-1}\Big(1 + \frac{1}{s}(\frac{F_\infty}{F_0} - 1)\Big) \qquad (5)$$

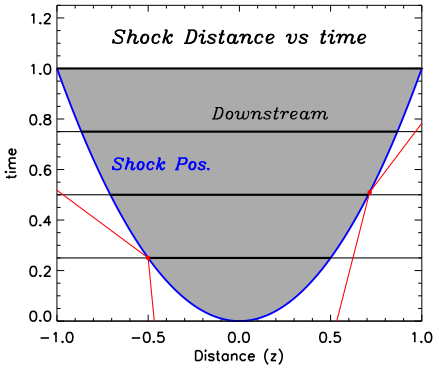

Fig. 3. Evolution of a field line after connecting the shock at $z = 0$ at time $t = 0$. The two connection-point moves away with decreasing speed. Also shown are a couple of scatter-free particle trajectories. Reflected particles move away from the decelerating shock (no multiple scattering)

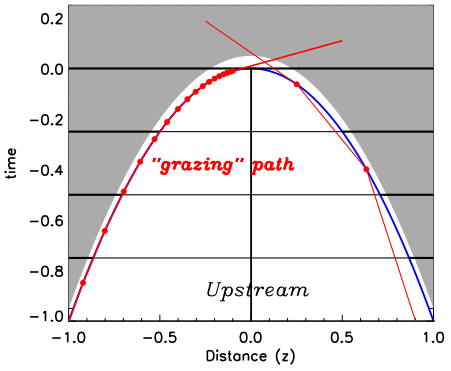

Fig. 4. Evolution of the shock connection on a field line detaching from the shock at $z = 0$ at time $t = 0$. Connection points run toward $x = 0$ with rapidly increasing speed. Sample trajectories of scatter-free are shown. Particles may be trapped in front of the shock and be accelerated by multiple mirroring as the shock site itself accelerates, and repeatedly catches the reflected particle.

which is softer than the 1-D case of $3s/(s-1)$.

The quantitative study of this possible softening will be addressed in future.

III. Acceleration at Perpendicular Shocks

Ideal, planar perpendicular shock are highly unlikely to occur. Instead, the curvature of the shock, together with the meandering of field lines leads to multiple intersection. Shock may have both large scale lateral structures, like the TS, [14],[7],[4] as well as smaller scale ripples [8]. Typically, shocks are perpendicular momentarily when the shock first hits a field line, and remain quasi-perpendicular for some time after [18]. Another obvious example is the time the field line is about to disengage the shock.

In this section we discuss what happens when a field line hits or disconnects a curved shock. The approach we adopt is following the history of one field line. We consider one field line with two points of discontinuity running away from the point of first contact or converging toward the point of last contact. As a simplification, we assume purely field aligned transport, which would correspond to massless particles. Effects of finite gyroradius, which eventually cause a breakdown at higher energies, will not be discussed here.

The two possible scenarios are depicted in Figures 3 and 4. Assuming a speed V_{sh} and a radius of curvature R_{curv} for the shock, one can readily calculate the motion of the two intersection point and obtain that $Z \propto t^{1/2}$, and

$$Z\frac{dZ}{dt} = Z\dot{Z} = V_{sh}R_{curv} = const. \qquad (6)$$

Field line may either just make contact with the shock or the may becoming disconnected from the shock. From the field line one sees two shock running away from the point of contact (Figure 3) or two shock converging to the point of disconnection (Figure 4). We note that $V = \dot{Z}$ is a projection speed, which can easily be very large.

The scenarios depicted in Figs. 3 and 4 can occur on both large and small scales. In the next subsections we discuss the two cases of diffusive description (when scattering maintains quasi-isotropy) an scatter-free motion (when the whole process is fast and scattering plays little role).

A. Diffusive Description

The scenarioss shown in Figs. 3 and 4 call for employing similarity variables. Instead of time, t, and distance, z, we use the shock-distance, $Z(t)$, and $\eta = z/Z$. In these variables the upstream and downstream equations take the form:

$$Z\frac{\partial f}{\partial Z} - \eta\frac{\partial f}{\partial \eta} = \frac{\partial}{\partial \eta}\Big(\frac{\kappa_{\|}}{ZV}\frac{\partial f}{\partial \eta}\Big) \qquad (7)$$

with matching condition to be applied at $\eta = 1$. The single important parameter is the dimensionless diffusion coefficient $\kappa_0 = \kappa_{\|}/(Z\dot{Z})$, which has (different) constant values both upstream and downstream. By contrast with the description in terms of t and z, eq. (7) avoids the singularity at $t = 0$. The 'expanding' case (Fig. 3) has the steady Z-independent solution

$$f(\eta, p) = Ap^{-\gamma}\int_{\eta}^{\infty} exp(-\eta^2/2\kappa_0)\, d\eta \qquad (8)$$

with

$$\frac{1}{\gamma(p)} = \frac{s-1}{3s}\int_{0}^{\infty} exp(-\eta(1+\kappa_0\eta/2))\, d\eta \qquad (9)$$

which, for small values of the upstream κ_0 can be approximated as $\gamma \approx 3s(1+\kappa_0)/(s-1)$, independently of the downstream value of κ_0. $\kappa_0 = 0$ returns the well-known 1-D exponent.

As for the case of 'converging' connection points (Fig. 4), $Z\dot{Z}$ turns negative. General solution is difficult go give since it shall depend on the starting time. We can show, however, that the total number of injected particles is turned into a power low spectrum

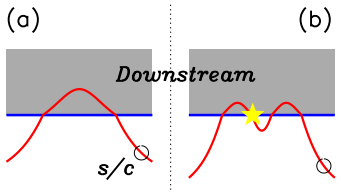

Fig. 5. Two possible field/shock configuration at a quasi-perpendicular shock, among which (b) may be significantly more efficient accelerator than (a). An observer on the right would see beamed events from the place marked with star.

of $\gamma = 3s/(s-1)$, independently from the upstream κ_0, provided that downstream diffusion is small.

B. Scatter-free Transport

Next we address the other extreme, the scatter-free case, which may apply on smaller scales, when the whole acceleration process is fast. The 'expanding' case, when the shock hits the field line, turns out less efficient. First, reflection can occur only after the shock slowed down enough to a speed comparable to the particle speed. Second, if reflection occurs, mirrored particles run away from the decelerating shock, giving no chance for multiple reflection.

The 'converging' case, on the other hand, is more interesting and turns out quite effective. Similar cases have been studied [10], [11], [12], [13], [19]. Here we suggest that the curvature of the shock plays an essential role in providing a mechanism that can lead to rapid and acceleration to high energies via multiple mirroring. This process is illustrated in Figure 4. A particle, which initially moves only slightly slower than the shock, can be reflected many times, since the shock moves faster and faster and overtakes the particle again and again.

The nonrelativistic case can be followed analytically. If, at the first encounter, the shock moves at a speed, V_1 and the particle moves a little slower at $w_\parallel$, then the particle is reflected and overtaken again. The next encounter happens when the shock moves at speed, V:

$$V/V_1 = w_\parallel/(2V_1 - w_\parallel) \tag{10}$$

We find that a grazing particle will be accelerated to

$$w^2_{\parallel,acc} \approx (s-1)\frac{w^2_\perp V_1^2}{(V_1 - w_\parallel)^2} \tag{11}$$

where $w_\parallel$ and $w_\perp$ refer to parallel and perpendicular particle speed at injection. Clearly, this process increases $w_\parallel$, thus producing a narrow beam in the forward direction. A breakdown is anticipated at high energies when gyroradius increases and the zero-radius approximation no longer applies.

We emphasize that important mechanism is not bouncing between the two shocks, but quasi-trapping in front of one accelerating shock. Figure 5 shows two possible field line configurations at a shock. Among these (b) is expected to be significantly more efficient in accelerating particles rapidly to high energies, and an observer sitting to right is more likely to see beamed particle events in case (b) from the place marked with star. If this is correct, this may add to the large variability of shock acceleration. This mechanism may be at work at several shocks, including the termination shock, interplanetary shocks, CME-driven shocks, or at astrophysical shocks.

Finally we note that the process may apply for fast moving electrons, whose acceleration in meandering field was discussed by [20]. The process we suggest here differs from [20] inasmuch that acceleration occurs by many reflectionion at one intersection by contrast with traversing many intersections.

IV. CONCLUSIONS

We considered particle acceleration at 2-D shocks. We presented a simple example to demonstrate that 'hot' and 'cold' regions are expected to form along the shock face, and that the flux of accelerated particles (even the average flux) should increase beyond the shock.

We addressed the formation of perpendicular shocks when curved shock engage or disengage a field line. We suggest that a very fast and effective acceleration can occur when particles are trapped in front of the accelerating and ever faster moving discontinuity. This acceleration mechanism is conceivably important at several solar, heliospheric, and astrophysical shocks.

V. ACKNOWLEDGEMENTS

The author benefited from discussions with J.R. Jokipii and J. Giacalone. This work was supported by NASA under grants NNX07AH19G, NNX09AB13G, and NNX08AQ14G, and by NSF under grant ATM-0641600.

REFERENCES

[1] E.C. Stone at al, *Science*, **309**, 2017 (2005).
[2] E.C. Stone at al, *Nature* , **454**, 71 (2008)
[3] J. Kóta and J.R. Jokipii, *AIPC 719*, 272 (2004).
[4] D.J, McComas and N.A. Schwadron, *Geophys. Res. Lett.*, **33**, 4102, (2006).
[5] J. Kóta and J.R. Jokipii, *AIPC 858*, 171 (2006).
[6] J. Kóta and J.R. Jokipii, *AIPC 1039*, 397 (2008).
[7] J.R. Jokipii, J. Giacalone, and J. Kóta, *Astrophys. J.* **611**, L141 (2004).
[8] M. Neugebauer and J. Giacalone, *J. Geophys. Res.* **110**, 12106 (2005).
[9] J. Giacalone and M. Neugebauer, *Astrophys. J.*, **673**, 629 (2008).
[10] G. Erdős, & A. Balogh, *Planet. Sp. Sci*, **38**, 343 (1990).
[11] R.B. Decker, *J. Geohys. Res*, **95**, 1199 (1990)
[12] R.B. Decker, *J. Geohys. Res*, **98**, 33 (1993)
[13] J. Giacalone, *Astrophys. J.* **624**, 316 (2005).
[14] G.P. Zank,*Space Sci. Rev.*, **89**, 413 (1999).
[15] N.A. Schwadron, M.A. Lee, and D.J. McComas, *Astrophys. J.*, **675**, 1584, (2006).
[16] J.R. Jokipii and J. Kóta, *AIPC 1039*, 390 (2008).
[17] E.N. Parker, *Planet. Sp. Sci*, **13**, 9, (1965).
[18] A.J. Tylka and M.A. Lee, *Astrophys. J.* **646**, 1319 (2006).
[19] D. Burgess, *Astrophys. J.* **653**, 316 (2006).
[20] J.R. Jokipii and J. Giacalone, *Astrophys. J.* **660**, 336 (2007).